J. Phys. B: At. Mol. Opt. Phys. **41** (2008) 015201 (7pp) doi:10.1088/0953-4075/41/1/015201

# The ionization of Mg by electron impact at 1000 eV studied by (e, 2e) experiments

**P Bolognesi[1], H Bohachov[2], V Borovik[2], S Veronesi[1,5], R Flammini[1], E Fainelli[1], A Borovik[2], J Martinez[3], Colm T Whelan[3], H R J Walters[4], A Kheifets[6] and L Avaldi[1]**

[1] CNR-IMIP, Area della Ricerca di Roma 1, Monterotondo Scalo, Italy
[2] Institute of Electron Physics, National Academy of Sciences, Uzhgorod, Ukraine
[3] Department of Physics, Old Dominion University, College of Sciences, Norfolk, USA
[4] Department of Applied Mathematics and Theoretical Physics, The Queen's University of Belfast, Belfast, UK
[5] Dipartimento di Chimica,Università degli Studi di Roma 'La Sapienza', Roma, Italy
[6] The Australian National University, Canberra ACT 0200, Australia

Received 18 July 2007, in final form 10 October 2007
Published 19 December 2007
Online at stacks.iop.org/JPhysB/41/015201

**Abstract**
The ionization of Mg 3s and 2p and He 1s has been studied in (e, 2e) experiments at about 1000 eV incident energy and 20 eV ejected electron energy for a momentum transfer between 0.5 and 2.1 au. The comparison with the predictions of the distorted wave Born approximation model shows a generally good agreement between experiment and theory. The differences observed between the He and Mg angular distributions can be explained as an initial state effect and are attributed to the differences between the He 1s and Mg 3s wavefunctions in the momentum space.

## 1. Introduction

The ionization processes from the valence shell of alkaline-earth atoms has attracted a lot of interest because just above the first ionization threshold, it displays strong deviation from the simple one-electron picture. This is due to the correlations between the two outer electrons, which after excitation may decay via autoionization producing resonance features in the ionization continuum. The series of these resonances have been studied in detail in both electron impact [1] and photoionization experiments [2]. Since Mg is a light, closed-shell atom it is also amenable by theories and several theoretical predictions of these series have been reported [2]. Less attention has been paid to the study of the direct ionization process by electron impact. The most complete way to fully characterize the dynamics of the ionization process of an atom by electron impact is to detect the scattered and ejected electrons in coincidence. The process can be written as

$$e_0(\vec{k}_0, E_0) + A \rightarrow A^+ + e_a(\vec{k}_a, E_a) + e_b(\vec{k}_b, E_b), \qquad (1)$$

where $(\vec{k}_0, E_0)$, $(\vec{k}_a, E_a)$ and $(\vec{k}_b, E_b)$ are the momenta and kinetic energies, respectively, of the incident, scattered and ejected electrons. A and $A^+$ represent the target atom and final ion respectively. The quantity that is measured in these experiments, known as (e, 2e) experiments, is the triple differential cross section (TDCS) $\mathrm{d}^3\sigma/\mathrm{d}\Omega_a\,\mathrm{d}\Omega_b\,\mathrm{d}E_a$, i.e. a cross section that is differential in the solid angles of the ejected and scattered electrons and in the energy of one of them. The energy of the second electron is determined by the energy conservation, $E_a + E_b = E_0 - \mathrm{IP}$, where IP is the ionization energy of the selected orbital of the target. (e, 2e) experiments have been successfully performed in rare gases under different kinematical conditions. The comparison of the results of these experiments with the theoretical predictions has provided valuable information to the present understanding of electron impact ionization [3]. Few (e, 2e) experimental investigations on Mg have been reported in the literature [4–7]. Pascual *et al* [4] investigated the momentum distribution of the 3s valence orbital. Murray [5] reported a set of experimental data for the ionization of the 3s valence shell of Mg and the outer shell of Na, K and Ca in coplanar symmetric geometry from threshold up to 67 eV above it. This work [5] provides a systematic comparison of the cross section among the different targets and with respect to He measured under the same energy conditions. The comparison with the theoretical predictions of distorted wave Born approximation (DWBA) and the convergent close

 

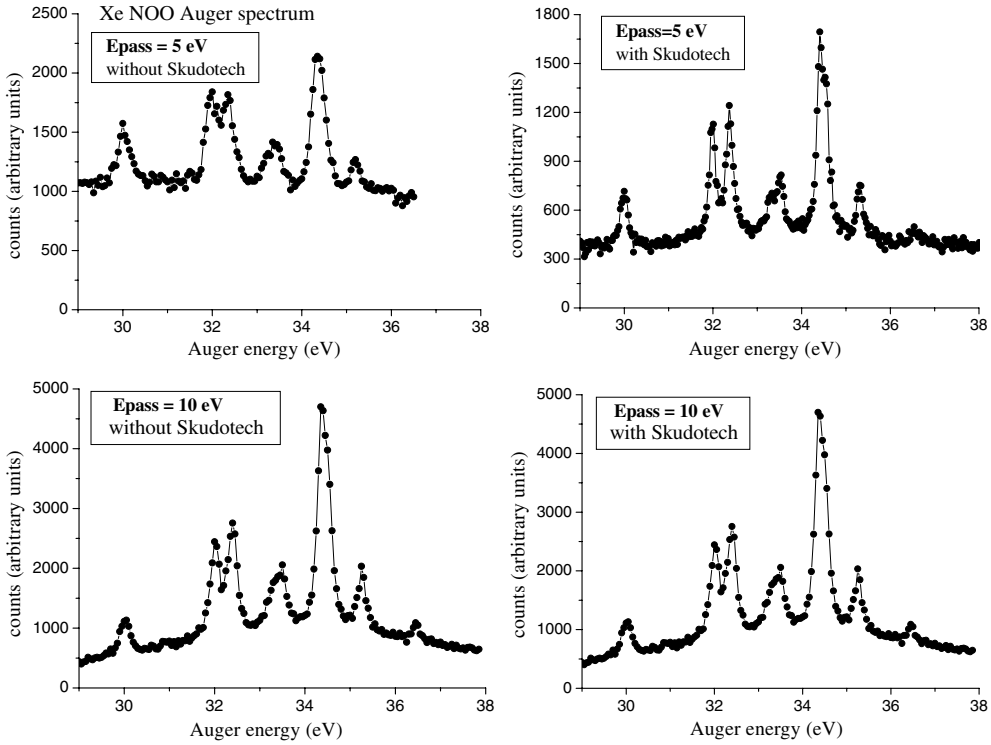


**Figure 1.** The Xe NOO Auger spectrum measured without (left panels) and with (right panels) the Skudotech shield, measured for two different pass energies for the electron analysers. The comparison between the two series shows the improvement in the energy resolution of the spectrometer due to a better compensation of the residual magnetic field.

coupling methods proved to be quite challenging because all the interactions which determine the reaction have to be treated on equal footing. van Boeyen *et al* [6, 7] investigated the role of the two-step mechanism in the single ionization process. To the purpose they performed a series of measurements of the ionization of the 3s, 2p and 2s shells of Mg at incident energy between 400 and 3000 eV and large momentum transfer $\vec{K} = \vec{k}_0 - \vec{k}_a$. Here we present the results of measurements performed on Mg 3s and He 1s at about 1000 eV incident energy, in unequal energy sharing ($E_a = 1000$ eV, $E_b = 20$ eV) and momentum transfer $K \leqslant 2.1$ au. The ionization of He in this dynamic regime is well understood; thus a comparison between the He and Mg data can provide valuable information on the correlation between the 3s valence electrons and the closed shells of the inner electrons both in the initial neutral and in the final ionic states. Indeed, assuming that the inner electrons remain unaffected by the ionizing collision the TDCS of Mg should be similar to that of He. In order to complete the description of the ionization of Mg, an (e, 2e) study of the 2p inner shell in one of the kinematics used for the experiment on the valence shell has been undertaken. All the experimental results have been compared with the predictions of the DWBA [8, 9], which satisfactorily described previous He data [10, 11].

The paper is organised as follows. Section 2 is devoted to the description of the experimental set-up and experimental procedure. The experimental results are presented in section 3, while the comparison with the theoretical models and some discussion are given in section 4. Conclusive remarks are collected in section 5.

## 2. Experimental details

A crossed-beam apparatus has been used to measure the ionization cross-section of Mg. The apparatus has been described in detail elsewhere [12]; here, only information relevant to the present measurements and the recent changes to the set-up will be reported. The vacuum chamber contains an electron gun, two twin 180° hemispherical electrostatic analysers, rotatable independently in the scattering plane, and a source for an atomic beam (a needle for rare gases and an oven in the case of Mg). In order to achieve a better compensation of the Earth's magnetic field, performed by three pairs of orthogonal square coils [12] external to the vacuum chamber, an internal 0.4 mm thick Skudotech shield has been installed. This substantially improved the energy resolution and transmission at the lowest pass energies in the analysers as shown in the case of the Xe NOO Auger spectra in figure 1.

The scattered/ejected electrons are analysed in energy by one of the two twin electron spectrometers. A three element zoom electrostatic lens focuses the electrons from the target region onto the entrance slit of the analyser. This is made by a hemispherical electrostatic deflector with 60 mm mean radius. The electrons, after angle and energy selection, are then detected by a channeltron multiplier. The output signals of the detectors are sent to the time to amplitude converter (TAC) through preamplifiers and constant fraction discriminators and finally stored in the computer via a multichannel analyser (MCA) card. The typical incident current, monitored by a Faraday Cup, was about 10 $\mu$A. A personal computer via a Labview software scans

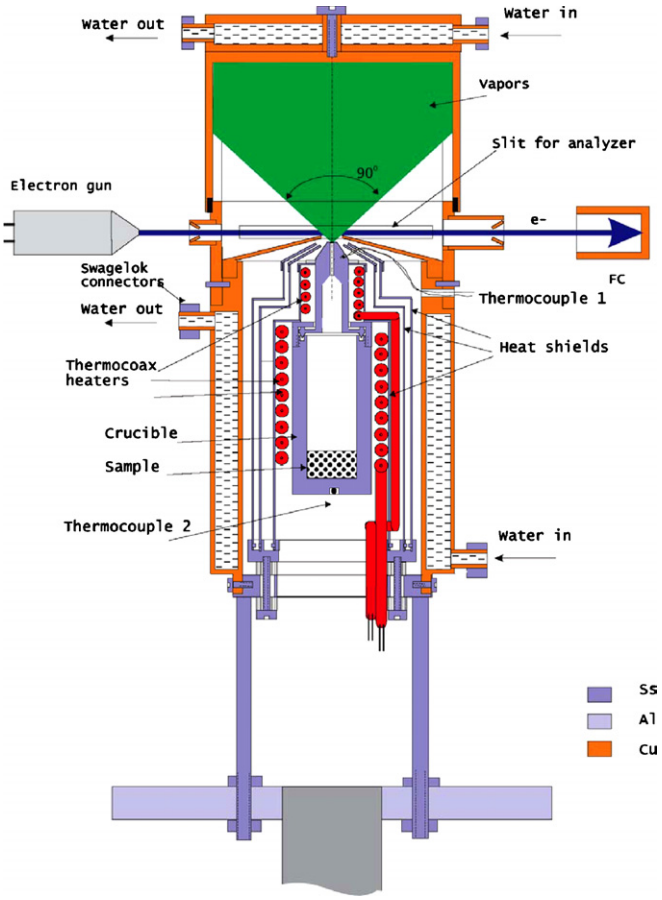


**Figure 2.** Schematic of the Mg oven.

the energy of the incident beam, changes the energy loss of the scattered electron, controls the movement of the turntables, sets the dwell time of the measurements, stores the non-coincidence and coincidence data and monitors the current of the beam during the measurements.

For these experiments the apparatus has been equipped with a resistively heated, anti-inductively wound oven, see figure 2.

Briefly, the oven source is composed of a stainless steel crucible where the top and the bottom parts can be independently heated to guarantee the gradient in temperature needed to avoid the blockage of the 10 mm long and 1 mm wide output nozzle. The setting and stability of the temperatures can be checked and monitored by means of the two independent *K*-type thermocouples. Crucible and heathers are enclosed in two concentric tantalum shields and then in a copper water-cooled jacket. This is equipped with a cylindrical 'cap' located above the interaction region and completely surrounding it, apart for suitable holes that allow the incident beam in/out of the scattering volume and two narrow slots in the scattering plane for the ejected/scattered electrons to reach the electrostatic analysers. These two slots allow the scattered angle $\theta_a$ to be varied from $-15$ (for the recoil momentum distribution measurements) to $+120^\circ$, while the ejected electron angle $\theta_b$ can be varied from 40 to $130^\circ$. This shielding of the interaction region prevented the contamination of the experimental apparatus from the Mg vapour. A separate hypodermic needle, running radially along the last copper conical shield, was used to admit calibration and tuning gases to the interaction region.

In practice, the oven was operated by exploiting only the upper heater to reach an operating temperature of about 400 °C. This procedure has the advantage to guarantee the needle part of the oven never to be cooler than the bottom one, preventing blockage of the output nozzle. Indeed, under these conditions we were able to run the Mg experiment continuously for more than a month, before some maintenance was required. No significant instability was observed. On the other hand, this procedure had the disadvantage that it required long time, about a day, for the heating up and cooling down of the crucible and to reach stable working conditions.

The energy $E_a$ of the scattered electrons has been fixed at 1000 eV, while ejected electrons with kinetic energy $E_b$ of 20 eV have been collected. Two types of measurements have been performed. In the first one, $\theta_a$-scan, the ejected electrons were collected at a fixed angle $\theta_b = 80^\circ$, while the angle $\theta_a$ of the scattered electrons was varied from $3^\circ$ to $14^\circ$. The value of $\theta_b = 80^\circ$ has been chosen in order to collect ejected electrons close to the direction of the momentum transfer in the ionizing collision. In the second kind of measurements the scattered electrons were detected at a fixed angle $\theta_a$, while the ejected electron angle $\theta_b$ was varied from $40^\circ$ to $130^\circ$. The collection efficiency of the ejected electron analyser has been calibrated on He by measuring the double differential cross section (DDCS) and comparing it to literature data [13]. The $\theta_a$ scale was calibrated by determining the symmetry of the scattered-electron DDCS around the incident beam direction. The energy resolution, full-width half-maximum (FWHM), in a coincidence energy spectrum was about 1.3 eV. Typical coincidence rates were of the order of 1–0.1 Hz for the Mg 3s and He 1s, and 2 mHz for the Mg 2p. In this work, only relative TDCSs have been measured. However, the scan in which $\theta_b$ is kept fixed and $\theta_a$ moves allowed us to establish a common scale of counts among all the measured Mg 3s and He 1s TDCS.

## 3. Results

The results of the measurements on Mg 3s and He 1s are shown in figures 3 and 4 respectively, while the TDCS of Mg 2p measured at $\theta_a = 7^\circ$ is displayed in figure 5.

In figure 3 the TDCSs measured in the $\theta_a$-scan for He and Mg are reported in the left and right panels, respectively. A noticeable difference in the behaviour of the TDCS is observed. While the He TDCS monotonically decreases as $\theta_a$ and therefore $K$ increases, the Mg one displays a well-defined maximum at about $\theta_a = 8^\circ$.

The TDCSs of He and Mg measured at $\theta_a = 5$, 7 and $12^\circ$ are shown in figure 4. The He TDCSs are in the left panel, while the Mg ones are in the right one. The TDCSs under asymmetric conditions ($E_a > E_b$ and $\theta_a \to 0^\circ$) are characterized [14] by the presence of two lobes. The first one, oriented nearly in the direction of $\vec{K}$, is associated with a binary collision of the incident electron, and it is indeed named the binary peak. The second peak, near the opposite direction,

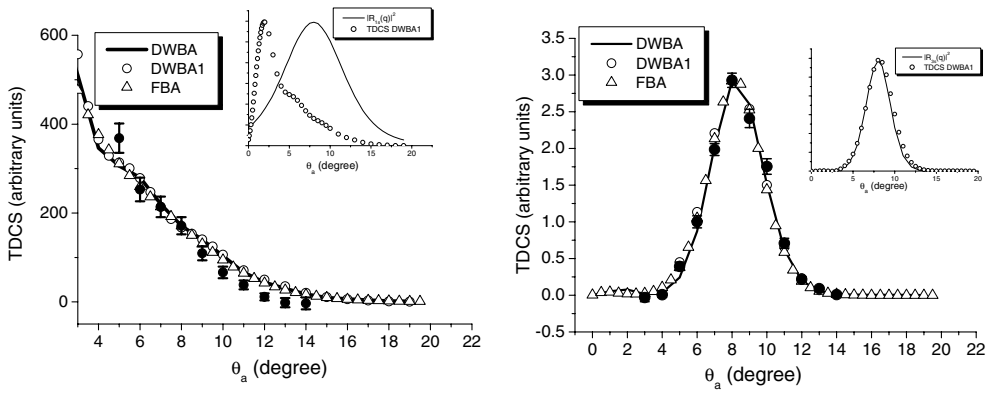


**Figure 3.** The TDCS of He 1s (left panel) and Mg 3s (right panel) measured by scanning the angle $\theta_a$ of the fast electron and detecting the slow electrons always at $\theta_b = 80^\circ$. The experiments (dots) are compared with the DWBA (black solid line), DWBA1 (open circles) and FBA (open triangle) calculations (see text). Theories and experiment are normalized at $\theta_a = 8^\circ$. The same normalization is also maintained in figure 4. In the insets, the DWBA1 theoretical TDCS (open circles) are plotted together with the momentum profile $|R_{ns}(q)|^2$ of the corresponding target orbital.

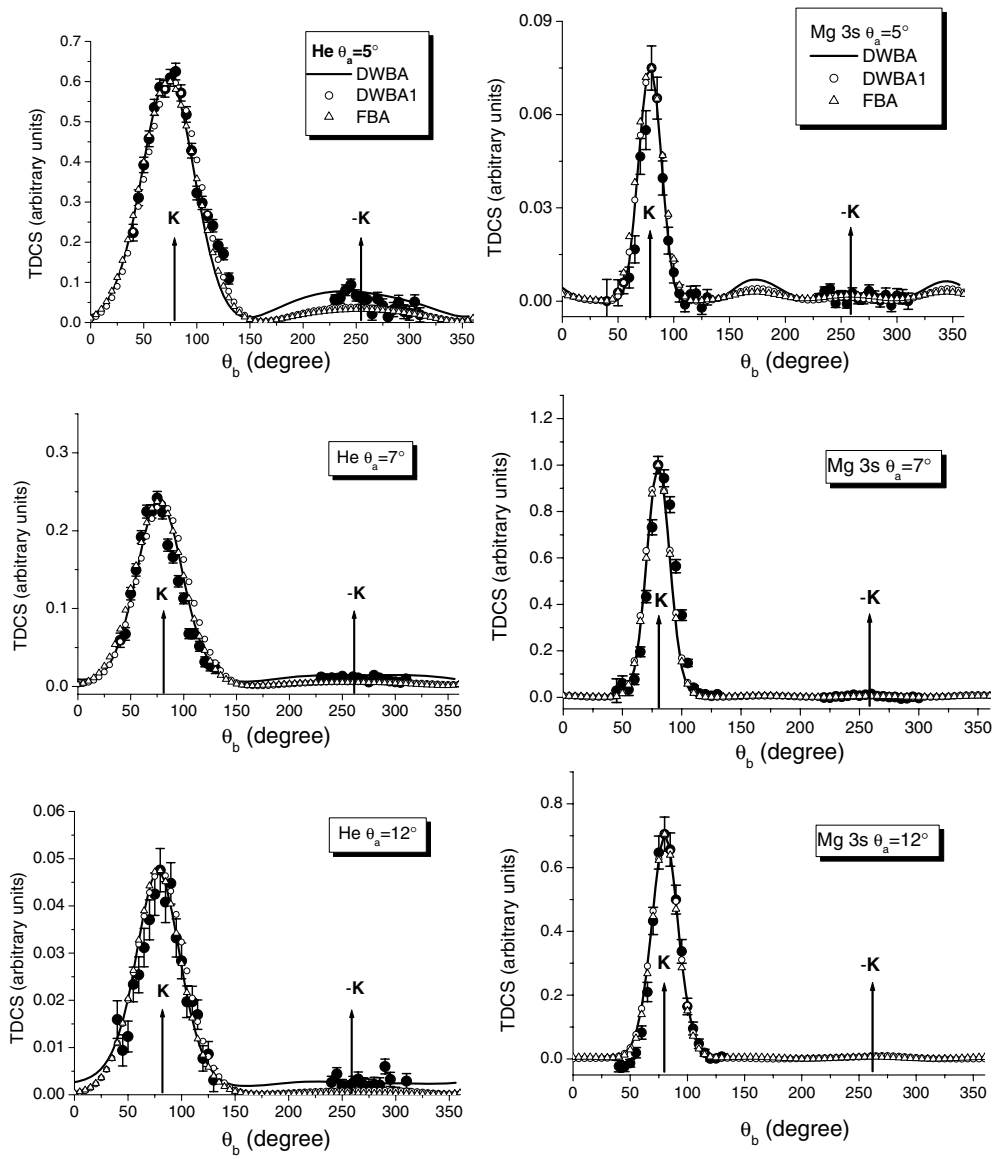


**Figure 4.** The TDCS of He 1s (left panels) and Mg 3s (right panels) at $\theta_b = 5$, 7 and $12^\circ$. The experiments (dots) are compared with the DWBA (black solid line), DWBA1 (open circles) and FBA (open triangle) calculations (see text). The same normalization of figure 3 between theories and experiment is used.

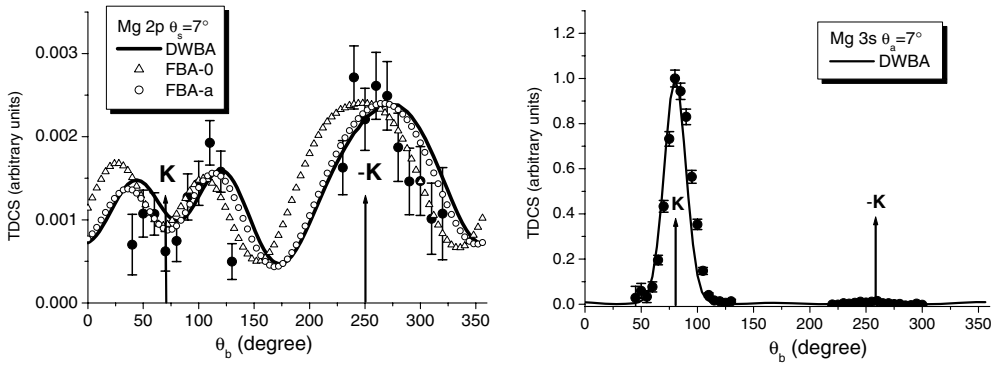


**Figure 5.** The TDCS of Mg 2p (left panel) and 3s (right panel) at $\theta_b = 7^\circ$. The experiments (dots) are compared with the DWBA calculations (solid line) and two calculations where either the incident electron (FBA-0, open triangle) or the scattered electron (FBA-a, open circle) are represented by plane waves.

is known as the recoil peak and it is commonly associated with a backscattering of the electrons on the atomic nucleus. The relative intensity of these lobes, their width and their position with respect to $\pm\vec{K}$ are the observables which provide the information on the dynamics of the ionizing process. In these measurements, we observe that in both He and Mg the centroids of the binary lobe are always, within the experimental uncertainty, in the direction of the momentum transfer. The width of this lobe that is always larger than 50° in He becomes about 30° in Mg. The binary-to-recoil ratio in He varies from 0.13 to 0.05 at $\theta_a = 5^\circ$ and 12°, respectively, while it is never larger than 0.04 in Mg.

The good agreement between the present He results and previous experiments under similar kinematic conditions [14] excludes major systematic errors in the present measurements.

In figure 5 the TDCSs of Mg 2p (left panel) and 3s (right panel) measured at the same energy of the scattered and ejected electrons and the same scattering angle $\theta_a = 7^\circ$ are compared. The experimental data have been normalized arbitrarily to the calculated cross section to achieve the best visual fit. At variance with the case of the 3s orbital, in the inner shell the recoil lobe is the dominant feature of the TDCS. Moreover, the binary lobe has a minimum near the $\vec{K}$ direction.

## 4. Discussion

The experiments have been compared with calculations performed in the DWBA. The TDCS for ionizing an electron from the (n, l) shell of a target atom is given by

$$\frac{\mathrm{d}^3\sigma}{\mathrm{d}\Omega_a\,\mathrm{d}\Omega_b\,\mathrm{d}E_a} \propto \frac{k_a k_b}{k_0} \times \sum_m [|f_{nlm}| + |g_{nlm}|^2 - \mathrm{Re}(f^*_{nlm} g_{nlm})]. \quad (2)$$

Here the sum over $m$ is a sum over the magnetic substates of the (nl) shell. $f_{nlm}(\vec{k}_a, \vec{k}_b)$ and $g_{nlm}(\vec{k}_a, \vec{k}_b)$ are the direct and exchange amplitudes for the ionization process, respectively. These amplitudes are given by

$$f_{nlm} = \langle \chi^-(\vec{k}_a, \vec{r}_a)\chi^-(\vec{k}_b, \vec{r}_b)|1/r_{ab}|\chi^+(\vec{k}_0, \vec{r}_a)\psi_{nlm}(\vec{r}_b)\rangle, \quad (3a)$$

$$g_{nlm} = \langle \chi^-(\vec{k}_a, \vec{r}_b)\chi^-(\vec{k}_b, \vec{r}_a)|1/r_{ab}|\chi^+(\vec{k}_0, \vec{r}_a)\psi_{nlm}(\vec{r}_b)\rangle. \quad (3b)$$

In equation (3), $\psi_{nlm}$ is the target bound-state wavefunction and $\chi^+$ and $\chi^-$ are distorted waves of the electrons in the initial and final states, with outgoing (+) and ingoing (−) scattered wave boundary conditions. The target wavefunction $\psi_{nlm}(\vec{r}) = R_{nl}(r)Y_{lm}(\vec{r}/r)$ is a product of the radial orbital and a spherical function. The radial orbital $R_{ns}(r)$ was found by solving a set of self-consistent Hartree–Fock equations [15]. In one implementation of the DWBA method, the incoming distorted wave $\chi^+$ was calculated in the static exchange potential of the neutral target. The outgoing distorted wave $\chi^-$ of the fast-scattered electron was calculated in both the static-exchange potential of the neutral atom and that of the singly charged final ion. The outgoing distorted wave $\chi^-$ of the slow ejected electron has been calculated in the static-exchange potential of the final ion state. Local exchange potentials of the Furness–McCarthy type [16] were used to simplify the static-exchange calculations. In an alternative implementation of the DWBA method (named DWBA1 in the figures), the distorted waves were calculated in the frozen core Hartree–Fock potential of the neutral or singly ionized target. In both implementations, the final state distorted waves are orthogonalized to the target orbital. Also, in order to better understand the physics of the process, first Born calculations where the incident/scattered electrons or both are described by plane waves have been performed. This means that the multiple scattering effects involving elastic scattering of the incident electron by the atom prior ionization or elastic scattering of the faster outgoing electron by the ion after the ionization are neglected.

In figure 3, the theoretical predictions and experiments have been normalized at $\theta_a = 8^\circ$. This scaling factor is the only free parameter used all over the comparisons between theory and experiment for both the TDCS of He 1s and Mg 3s reported in figure 4. The comparison between the calculations done using plane waves for the incident and scattered electrons, labelled FBA in figures 3 and 4, and the full DWBA1 shows that a description of the ejected electron as a Coulomb distorted wave is enough to account for the experimental observations. A general good agreement is found between theory in both variations and experiment in all the investigated kinematics for

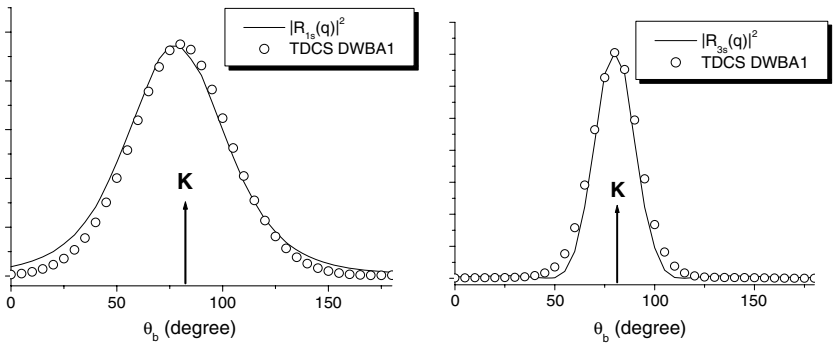


**Figure 6.** DWBA1 theoretical TDCS (open circles) of He 1s (left panels) and Mg 3s (right panels) at $\theta_b = 12^\circ$ plotted together with the momentum profile $|R_{ns}(q)|^2$ of the corresponding target orbital.

He 1s and Mg 3s. It has to be noted that the theory correctly describes not only the shapes of the measured TDCS, but also their relative intensities.

The absence of any appreciable shift of the binary lobes with respect to the $\vec{K}$ direction implies that models based on an approximation of the interaction at first order should satisfactorily account for the results. This is indeed confirmed by the calculations of the present work.

The main difference between He and Mg is observed in the shape of the TDCS in the $\theta_a$-scan. The energies of the scattered and ejected electrons are the same in both cases as well as the $\theta_a$ angular range. This excludes that the difference is due to a final state effect. The variation in the momentum transfer between the two measurements is negligible; thus, the difference cannot be attributed to the dependence of the TDCS on the momentum transfer. As a consequence, the observed difference has to be ascribed to the structure of the target, i.e. to the bound state initial wavefunction. In the hypothesis of a binary collision by momentum conservation, one can reconstruct the momentum $\vec{q} = \vec{k}_a + \vec{k}_b - \vec{k}_0$ of the ejected electron before the collision. In the present measurements, $q$ varies from almost 0 au at $\theta_a = 8^\circ$ to 0.6 and 0.9 at $\theta_a = 4^\circ$ and $14^\circ$. According to the measurements of the electron momentum distribution of the Mg 3s by Pascual *et al* [4], the probability to find in the Mg 3s orbital an electron with 0.6 au is vanishing. On the other hand, for the He 1s [17] case, this probability is only half of that to find an electron with $q = 0$ au. In other words, the Mg 3s momentum distribution is substantially narrower than the He one. Thus, while the trend of the He TDCS in figure 3 is mainly determined by its dependence on $K$, in the case of Mg the leading factor is the initial state wavefunction. This is clearly seen in the inset of figure 3, where we plot the TDCS along with the momentum profile $|R_{ns}(q)|^2$ of the corresponding target orbital. The same argument can be used to explain the narrower binary lobe in the Mg TDCS shown in figure 4. This is well accounted for by the theoretical models, which use a self-consistent field Hartree–Fock wavefunction [15] for the initial state. In figure 6, we plot the squared wavefunction of the target orbitals in the momentum space $|R_{ns}(q)|^2$ for He ($n = 1$, left) and Mg ($n = 3$, right) scaled to the corresponding DWBA TDCS in the region of the binary lobe. We choose the largest scattering angle of $\theta_a = 12^\circ$, which corresponds to the largest momentum transfer $K$. In the limit of very large $K$ and when both the scattered and ejected electrons can be represented by plane waves, the TDCS is directly proportional to the squared target orbital in the momentum space. This is the foundation of the electron momentum spectroscopy technique [18]. Although $K$ is quite modest in the present measurement and the low value of $E_b$ prevents the use of a plane wave for the description of the ejected electron, the momentum profile of the target orbital describes the shape of the TDCS quite well clearly indicating the difference between He and Mg. The small differences between the calculated TDCS and $|R_{ns}(q)|^2$ observed in figure 6 in the case of He at $\theta_b < 70^\circ$ can be ascribed to the too low $E_b$. The 1s electron of He is tightly bound in the coordinate space and has quite a broad momentum profile. In comparison, the 3s electron of Mg is shielded from the nucleus by valence electrons and has quite a diffuse orbital in the coordinate space resulting in a narrow momentum profile. The same effect can be observed in the TDCS of double photoionization of He and Mg [19].

The interaction of the electrons with the atomic nucleus plays a central role in the appearance of the recoil lobe. Thus, the strong depletion of this lobe in the Mg 3s TDCS with respect to the He ones can be explained by the fact that, being the 3s orbital a much more peripherical orbital than the He 1s, the probability of the involvement of a scattering on the nucleus in the ionization process is quite low and decreases faster than in He when $K$ increases.

The main features observed in the TDCS of the Mg 2p orbital are the split binary lobe and the dominance of the recoil lobe. These observations are in complete agreement with the results of previous (e, 2e) studies on inner shell ionization, for example in the case of Ar 2p [20–23]. The split binary lobe is due to the p character of the ionized orbital, whose momentum distribution is characterized by a node at $q = 0$. As clearly discussed in a recent paper by Kampp *et al* [24] in the PWBA, the $f$ direct scattering amplitude is proportional to the initial state wavefunction in momentum space. Thus, the TDCS follows the behaviour of the 2p momentum distribution which rises from $q = 0$ to a local maximum and then decreases monotonically as $q$ increases. The kinematics condition which allows us to achieve $\vec{q} = 0$ is called the bound Bethe ridge kinematics. Under such a condition in a plane wave calculation, a zero in the TDCS is expected. This zero becomes a minimum of the TDCS

when distortion effects, needed for example to describe a low energy ejected electron, are taken into account [24]. The main effect of the distortions is a shift with respect to the $\vec{K}$ direction towards larger $\theta_b$. Then if the kinematics does not comply with the bound Bethe ridge condition and $\vec{q} = 0$ is not reached in the experiment, a minimum may still exist in the TDCS. This is exactly the situation of the present experiment where at $\theta_b = 70°$, the minimum $q$ value ($q = 0.1$ au) is reached and the TDCS displays a minimum as well (figure 5). The large increase of the recoil lobe, mainly observed when the ejected electron energy is smaller than the inner-shell binding energy, has been investigated in Ar both experimentally and theoretically [22]. It has been attributed to two factors. The first one is a double-scattering process in which the incident electron backscatters elastically off the nucleus and then ionizes the target and the second one is the strong final state interaction between the slow ejected electrons with the nucleus. Both effects are included implicitly in the present DWBA calculation through the distorted waves of the electrons, and the DWBA calculations satisfactorily describe the experimental results. The comparison with two other first Born calculations whether either the incident electron (FBA-0) or the scattered one (FBA-a) is described by plane waves clearly indicates the key role of the description of the incident electron in inner shell ionization. Indeed the FBA-0 calculation predicts a TDCS which is symmetric with respect to the $\vec{K}$ direction, while the DWBA and FBA-a consistently with the experiment predict a TDCS shifted towards larger $\theta_b$. These effects, already observed in the study of the inner shells of Ne and Ar [23], stem from the strong static potential of 'heavy' atoms, which is particularly important in inner shell ionization since the ionization process occurs close to the nucleus, where the static potential is at its strongest [23].

## 5. Conclusions

The TDCSs of Mg 3s and 2p orbitals have been measured at about 1000 eV incident energy and 20 eV ejected electron energy for a range of momentum transfer between 0.5 and 2.1 au.

The experimental results of Mg 3s have been compared with the TDCS of He 1s measured in the same kinematics and with the first Born calculations which use different combinations of plane and distorted waves to describe the incident, scattered and ejected electrons. A good agreement between experiment and theory is found in all the investigated kinematics of He 1s and Mg 3s provided a distorted wave is used for the description of the ejected electron. The most interesting observation is that in these kinematics, the characteristics of the 3s initial state wavefunction determine the main features of the Mg TDCS.

The inner shell measurement confirms the general trend observed in the previous studies in rare gases. The large recoil structure, which dominates the angular distribution, is mainly due to multiple scattering effects which appear to be well accounted for by the present DWBA calculations. It would be interesting to increase the energy of the slow ejected electron close to that of the Auger electrons (∼35 eV) emitted in the relaxation of the 2p hole. In such a case, the indistinguishability of the two electrons might lead to intriguing interference effects that may challenge the present theoretical models for (e, 2e) inner shell studies.

## Acknowledgments

This work is supported by the INTAS Research Project 'Dynamics of correlated particles in the continuum', no 03-51-4706, and the MIUR FIRB project 'Probing the microscopic dynamics of chemical reactivity'.

## References

[1] Rassi D, Pejčev V, Ottley T W and Ross K J 1977 *J. Phys. B: At. Mol. Phys.* **10** 2913
[2] Wehlitz R, Lukic D and Juranic P N 2007 *J. Phys. B: At. Mol. Opt. Phys.* **40** 2385 and references therein
[3] McCarthy I E and Weigold E 2005 *Electron-Atom Collisions* (Cambridge: Cambridge University Press)
[4] Pascual R, Mitroy J, Frost L and Weigold E 1988 *J. Phys. B: At. Mol. Opt. Phys.* **21** 4239
[5] Murray A J 2005 *Phys. Rev.* **A72** 062711
[6] van Boeyen R W, Doering J P, Moore J H, Coplan M A and Cooper J W 2002 *J. Phys. B: At. Mol. Opt. Phys.* **35** L97
[7] van Boeyen R W, Watanabe N, Cooper J W, Doering J P, Moore J H and Coplan M A 2006 *Phys. Rev.* **A73** 032703
[8] Madison D H, Calhoun R V and Shelton W N 1977 *Phys. Rev.* **A16** 552
[9] Whelan C T, Allan R J, Walters H R J and Zhang X 1993 *(e, 2e) and Related Processes* ed C T Whelan, H R J Walters, A Lahmam Bennani and H Ehrhardt (Dordrecht: Kluwer) p 1
[10] Zhang X, Whelan C T and Walters H R J 1990 *J. Phys. B: At. Mol. Opt. Phys.* **23** L509–16
[11] Zhang X, Whelan C T and Walters H R J 1990 *J. Phys. B: At. Mol. Opt. Phys.* **23** L173–8
[12] Avaldi L, Camilloni R, Multari R, Stefani G, Zhang X, Walters H R J and Whelan C T 1993 *Phys. Rev.* A **48** 1195
[13] Kim Y K 1983 *Phys. Rev.* A **28** 656
[14] Avaldi L, Camilloni R, Fanelli E, Stefani G, Franz A, Klar H and McCarthy I E 1987 *J. Phys. B: At. Mol. Opt. Phys.* **20** 5827
[15] Chernysheva L V, herepkov N A and Radojevic V 1976 *Comp. Phys. Commun.* **11** 57
[16] Furness J B and McCarthy I E 1973 *J. Phys. B: At. Mol. Phys.* **6** 2280
[17] Lahmam-Bennani A, Avaldi L, Stefani G and Fainelli E 1988 *J. Phys. B: At. Mol. Opt. Phys.* **21** 2415
[18] Weigold E and McCarthy I E 1999 *Electron Momentum Spectroscopy* (New York: Kluwer)
[19] Kheifets A and Bray I 2007 *Phys. Rev.* A **75** 042703
[20] Lahmam-Bennani A, Wellenstein H F, Duguet A and Daoud A 1984 *Phys. Rev.* A **30** 1511
[21] Bickert P, Hink W, Cappelo C D and Lahmam-Bennani A 1991 *J. Phys. B: At. Mol. Opt. Phys.* **24** 4603
[22] Cavanagh S and Lohmann B 1997 *J. Phys. B: At. Mol. Opt. Phys.* **30** L231
[23] Zhang X, Whelan C T, Walters H R J, Allan R J, Bickert P, Hink W and Schönberger S 1992 *J. Phys. B: At. Mol. Opt. Phys.* **25** 4325–35
[24] Kampp M, Roche P J P, Whelan C T, Madison D H, Rasch J and Walters H R J 2002 *J. Phys. B: At. Mol. Opt. Phys.* **35** 2325